Simulation of Fluid Flow in a High Compression Ratio Reciprocating Internal Combustion Engine

G Sridhar*, P J Paul and H S Mukunda
Combustion, Gasification and Propulsion Laboratory, Department of Aerospace Engineering, Indian Institute of Science, Bangalore, India

The MS was received on 1 November 2003 and was accepted after revision for publication on 21 April 2004.

* Corresponding author: Combustion, Gasification and Propulsion Laboratory, Department of Aerospace Engineering, Indian Institute of Science, Bangalore 560012, India.

Abstract: This paper discusses the detailed three-dimensional modelling of a reciprocating engine geometry comprising a flat cylinder head and a bowl-in-piston combustion chamber, simulating the motoring or non-firing conditions. The turbulence is modelled using a standard k–1 model and the results are compared against experimental results from the literature. Computed velocity profiles at time steps close to top centre (TC) are presented. The effect of squish and reverse squish becomes significant in a high compression ratio reciprocating engine. This enhanced fluid movement during a reverse squish regime could have an effect on burn rate, particularly in a spark ignition engine fuelled with biomass-derived producer gas, which has optimum ignition timing close to TC.

Keywords: computational fluid dynamics, compression ratio, squish, reverse squish, turbulence

NOTATION

ABC	after bottom centre
BBC	before bottom centre
BC	bottom centre
BTC	before top centre
B	body force
CA	crank angle
CFD	computational fluid dynamics
CR	compression ratio
DNS	direct numerical simulation
H	total enthalpy
k	turbulence kinetic energy
lı	integral length scale
LES	large eddy simulation
p	pressure
p–u	pressure–crank angle
RSV	reverse squish velocity
R	characteristic gas constant
S	separation zone
t	time
T	torroidal structure
TC	top centre
TKE	turbulence kinetic energy
T	Temperature
u′	turbulence intensity
U	velocity
x	coordinate
a	crank angle
1	turbulence dissipation rate
l	thermal conductivity
m	viscosity
r	density
s	stress tensor

1 INTRODUCTION

Turbulence in reciprocating engines is considered important because of its large influence on the combustion characteristics. In order to find optimum conditions in a combustion system, it is essential to obtain a good approximation of the in-cylinder turbulence. From this viewpoint, multidimensional modelling using computational fluid dynamics (CFD) codes is pursued and involves simulation with and without combustion. One of the major challenges of CFD in recent times has been that several models need to be combined in order to simulate a complete engine cycle. The k–ε model is the most commonly used turbulence model in CFD, even though its deficiencies are known [1]; indeed, the k–ε model is still considered to the best compromise between computational time and precision. However, in recent times, second-order closure models

have been pursued in engine modelling [2, 3], with increased validity of the model. However, complex numerical approaches such as direct numerical simulation (DNS) are difficult to implement in engine-like situations because of enormous prerequisites such as high mesh density and exorbitant CPU time. This is also the case with large eddy simulation (LES), where accurate subgrid models are required, and research in this field is still in progress [2]. For implementation of the CFD model, mesh density assumes primary importance; some of the earlier studies on engine geometry using different mesh densities are summarized in Table 1.

From Table 1 it is evident that computational mesh densities have increased with enhancement in computational speed over a period of two decades. Reasonably good qualitative (and in a few cases quantitative) comparison has been claimed by the some of the researchers listed above, with a mesh density less than 0.12 million cells, by using turbulence models such as k– ε in most cases and a second-order closure model in one case [2]. They claim that a grid-independent solution based on global balances in momentum and kinetic energy with mesh refinement has little effect on the results.

In the present work, a detailed three-dimensional cold flow study is conducted on piston engine geometry with a mesh density of 0.2 million cells to simulate the engine cold flow condition. CFD simulation is conducted over two complete motoring cycles involving intake, compression and expansion and exhaust processes on bowlin-piston engine geometry at two compression ratios (CRs), 17.0 and 11.5. Data on the turbulence parameters and reverse squish velocities (referred as the reverse squish period at the beginning of the expansion process) derived from the above study have been used as input in the zero dimensional modelling. This aspect has been demonstrated by the present authors in earlier publications [13, 14]. The simulation is conducted using a commercial CFD code CFX-4.3. The grid is generated using a preprocessor called CFX-build. The numerical solution is obtained using CFXsolver, which is based on a finite volume technique. The results are analysed using a post-processor known as CFX-analyse.

Reasearcher	Summary of work	Geometry and mesh
Schapertons and Thiele [4]	Cold flow studies in two different bowl-in-piston geometries of adiesel engine	Engine cylinder, 0.02 million cells
Haworth et al. [5]	Cold flow studies with different intake valves and limited comparison with experimental results	Intake pipe and engine cylinder, 0.023 million cells
Trigui et al. [6]	Cold flow studies using STAR-CD code; experimental flowfield data used as initial conditions	Engine cylinder, 0.06 million cells
Jones and Junds [7]	Cold flow in a four-valve pent roof SI engine through two complete cycles using SPEED code. Predictions compared qualitatively and quantitatively (one case) with the experimental results	Engine cylinder, 0.03 million cells
Strauss et al. [8]	Simulation of combustion in an indirect combustion chamber geometryof a diesel engine using SPEED codes	Engine cylinder, 0.0425 million cells
Reuss et al. [9]	Cold flow studies compared against particle image velocimetry resultsusing KIVA and GMTEC codes	Engine cylinder, 0.06 million cells
Khalighi et al. [10]	Flow and combustion modelling in a four-valve SI engine. Cold flow results compared with water-analogue flow studies. Numerical inaccuracies discussed	Engine cylinder, 0.023–0.12 million cells
Lebrere and Dillies [2]	Cold flow using the k–1 and second-order closure turbulence model. Predictions compared against LDA measurements	Engine cylinder, 0.072 million cells
Bauer et al. [11]	Flow through the intake system of an SI engine using STAR-CD code. Predictions of instantaneous pressure and temperature in the intake system compared with the experimental results	Intake system and engine cylinder, 0.12 million cells
Duclos et al. [12]	Simulation of SI engine combustion using KIVA-II code and compared with the experimental results	Intake pipe and engine cylinder, 0.12 million cells

2 PROBLEM DEFINITION

The geometry considered for modelling is the combustion chamber geometry of a gas engine, which is converted from a production diesel engine. The combustion chamber comprises a flat cylinder head and an eccentrically located hemispherical bowl. The engine cylinder measures 110 mm in diameter _ 116 mm in stroke, and the hemispherical bowl is 30 mm in radius. The other technical details of the engine are dealt with in earlier publications [13, 15]. The piston, which is one of the moving boundaries, simulates the reciprocating movement of an engine. The minimum clearance between the piston and the cylinder head as the piston approaches its uppermost point of travel is about 1.5 mm for a CR of 17.0 and increases to 5.2 mm at a CR of 11.5. The other moving boundary is formed by the intake valve (non-swirl type) to allow fluid flow into the cylinder geometry. The geometry is also provided with an exhaust port that is opened at an appropriate time to simulate the exhaust process. Since the simulation does not involve combustion, simplifying the geometry with a port in place of a moving exhaust valve is taken not to influence the accuracy of the results.

The geometry described above is relatively complex, involving a time dependent grid to simulate the piston and intake valve movement. This is achieved by writing additional Fortran programs to simulate the transient grid in the present study. Simulation is also conducted on a flat piston (without the bowl) at a CR of 17.0 in order to assess the magnification of turbulence intensity caused by the presence of the bowl.

3 GRID GENERATION

The geometry described in a Cartesian coordinate system is required to simulate the reciprocating engine operation. This is achieved using a multiblock grid methodology, in which a set of unstructured blocks is glued together, and each of which is a structured grid. In the resulting geometry with a three-block structure, it is found that there is a mismatch of the grids at the interfacing planes. These are resolved by identifying the interfacing nodes of the adjacent blocks as 'unmatched' and thereby allow the solver to adopt appropriate methodology for data transfer between the adjacent blocks.

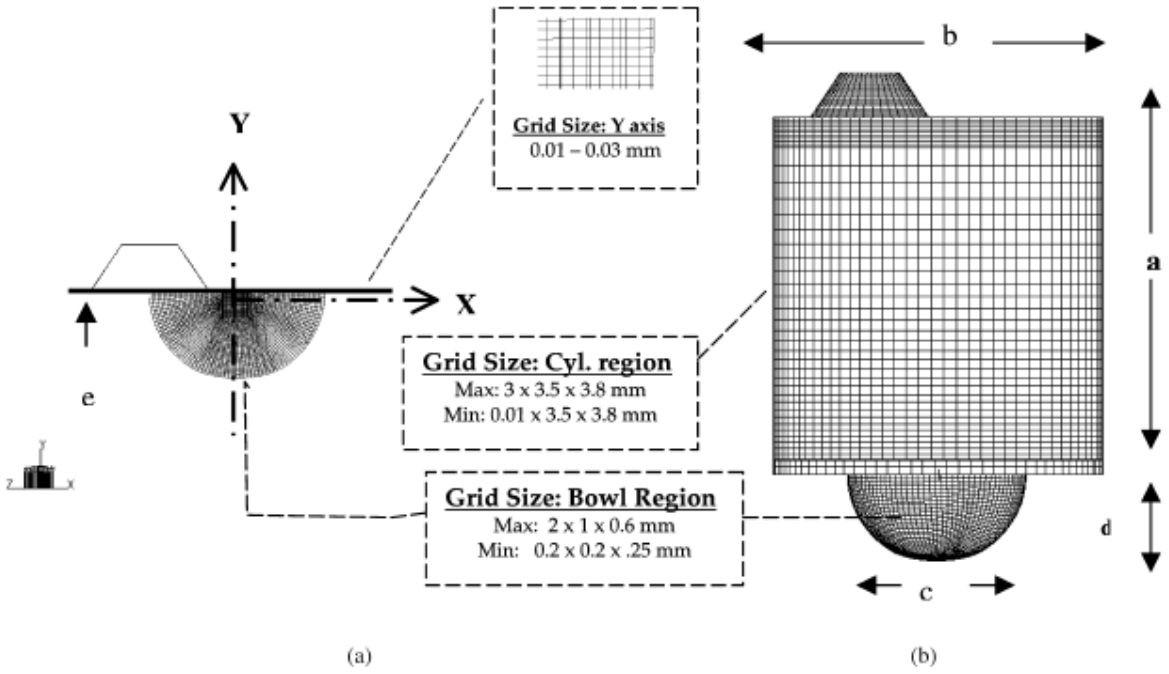

Fig. 1 Grid distribution (a) with the intake valve fully closed and the piston at TC and (b) with the intake valve fully open and the piston at BC: a = 116 mm; b = 110 mm diameter; c = 60 mm diameter; d = 30 mm and e=1.5/5.2 mm for CR = 17.0/11.5

Also, suitable regions are identified as 'patches' in order to define the boundary conditions. The type of grid adopted for this geometry is 'two-way bias'. In this approach, the grid density increases from the central region towards the walls. The grid distribution with the piston at extreme positions is shown in Fig. 1. When the piston is at bottom centre (BC), the minimum and maximum grid sizes are 0.01 and 3.0 mm in the axial direction and 3.5 mm in the radial direction, and the azimuthal spacing is about 4.08.

Similarly, when the piston is at top centre (TC), the change in the grid size occurs only in the axial direction and corresponds to a minimum and maximum of 0.01 and 0.03 mm respectively. This grid pattern corresponds to a mesh density of 0.2 million computational nodes. The geometry is created with the piston at TC and the intake valve fully closed, as shown in Fig. 1a. Furthermore, the intake and the piston move in accordance with the engine cycle operation to simulate different processes.

4 BOUNDARY AND INITIAL CONDITIONS

The flow domain considered for simulation is downstream of the engine intake manifold. Therefore, flow through the intake manifold is not modelled. However, the transient flow condition in the intake manifold is accounted for by introducing a time-varying boundary condition (pressure) at the intake valve. The manifold pressure profile is generated from the actual pressure measurements on the engine. These are obtained using a strain gauge transducer mounted on the intake manifold, very close to (upstream of) the intake valve of the cylinder, with the engine operating at rated speed (1500 r/min). Similarly, intake valve movement is simulated using the actual valve lift profile of the engine. In the computations, a minor change in the intake valve opening timing is introduced in order to simplify the grid movement. The intake valve opens at TC instead of actually opening a few degrees [26° crank angle (CA)] earlier. Similarly, the closure of the exhaust port occurs at TC. The valve overlap period is thus not simulated, and it is expected not to affect the predictions since the simulation does not involve combustion. The complete closure of the intake valve is simulated by giving the grid size at the valve region a low value (< 0.25 mm) and subsequently imposing a wall condition. The boundary conditions for the turbulence equations have been specified using traditional wall functions (see reference [16]).

The computations commence with the induction process in which a set of initial conditions is assumed for the first cycle. Initial conditions for some of the variables are obtained from motored zero-dimensional results, namely initial pressure and temperature. The initial conditions correspond to a pressure of 920 kPa (corresponding to atmospheric pressure at Bangalore) and a temperature of 300 K for the working fluid (air). However, suitable assumptions are made of the remaining variables. The three components of velocity are taken as 0.001 m/s; similarly, initial low values for turbulence kinetic energy and dissipation rate are assumed at 0.001 m^2/s^2 and 0.001 m^2/s^3 respectively. A constant wall temperature of 450 K is considered throughout the simulation. The working fluid is treated as a single gas since combustion is not considered. These computations are repeated over two complete cycles in order to obtain results independent of the initial conditions.

5 ASPECTS OF MODELLING

The CFD code solves the three-dimensional, ensembl eaveraged Navier–Stokes and enthalpy equations governing turbulent and compressible gas flow along with heat transfer for the geometry described above. To simulate the turbulence parameters, a standard k– ε model has been chosen without and with compressibility effects due to velocity dilatation. The working fluid is treated as a single gas since combustion is not simulated. The algorithms employed for spatial and temporal discretization are first-order accurate hybrid and backward difference schemes respectively. The governing equation set includes the continuity equation, three momentum equations, the enthalpy equation and two turbulence equations.

For flow calculations with a moving grid, the transport equations are suitably modified [17]. There are two main changes: the transient term allows for the change in volume and the advection terms include the grid velocity. The complete sets of equations are as follows

$$\frac{1}{\sqrt{g}}\frac{\partial\sqrt{g}\rho}{\partial t}+\nabla\left[\rho\left(U-\frac{\partial x}{\partial t}\right)\right]=0 \quad (1)$$

$$\frac{1}{\sqrt{g}}\frac{\partial\sqrt{g}\rho U}{\partial t}+\nabla\left[\rho\left(U-\frac{\partial x}{\partial t}\right)\otimes U\right]=B+\nabla\sigma \quad (2)$$

$$\frac{1}{\sqrt{g}}\frac{\partial\sqrt{g}\rho H}{\partial t}+\nabla\left[\rho\left(U-\frac{\partial x}{\partial t}\right)H\right]-\nabla(\lambda\nabla T)=\frac{\partial p}{\partial t}-\nabla\rho\frac{\partial x}{\partial t} \quad (3)$$

where g accounts for the expansion and compression of the grid, x is the grid position, U is the velocity, H is the total enthalpy, B is the body force, λ is the thermal conductivity and σ is the stress tensor. Similar transformation is applied for the turbulent transport equations. The transport equations for turbulence kinetic energy, k, and turbulence dissipation rate, ε are as follows. The equation for k is given by

$$\frac{\partial\rho k}{\partial t}+\nabla(\rho U k)-\nabla\left[\left(\mu+\frac{\mu_T}{\sigma_k}\right)\nabla k\right]=P-\rho\varepsilon \quad (4)$$

where P is the shear production defined as

$$P=\mu_{\text{eff}}\nabla U[\nabla U+(\nabla U)^T]-\frac{2}{3}\nabla U(\mu_{\text{eff}}\nabla U+\rho k) \quad (5)$$

The equation for ε without the compressibility effect is given by

$$\frac{\partial\rho\varepsilon}{\partial t}+\nabla(\rho U\varepsilon)-\nabla\left[\left(\mu+\frac{\mu_T}{\sigma_\varepsilon}\right)\nabla\varepsilon\right]=C_1\frac{\varepsilon}{k}P-C_2\rho\frac{\varepsilon^2}{k} \quad (6)$$

The equation for ε with the compressibility effect is given by

$$\frac{\partial\rho\varepsilon}{\partial t}+\nabla(\rho U\varepsilon)-\nabla\left[\left(\mu+\frac{\mu_T}{\sigma_\varepsilon}\right)\nabla\varepsilon\right]=C_1\frac{\varepsilon}{k}P-C_2\rho\frac{\varepsilon^2}{k}+C_3\rho\varepsilon\nabla U \quad (7)$$

where μ is the molecular viscosity, μ_T is the turbulence viscosity and s is the Prandtl number. The values of the constants are C_1=1.44, C_2 = 1.92 and C_3 =20.373. The constants C_1 and C_2 are the standard constants used in the k- ε model. The value considered for C_3 is the same as that of Jennings [18].

Since the flow is considered to be compressible, the equation of state is the ideal gas law given by

$$P=\rho RT \quad (8)$$

6 COMPUTATIONAL PROCEDURE

Computations have been made for an operational speed of 1500 r/min, with a time step of the order of 0.5° CA (50 ms). The calculations commence with the piston at TC, with the intake valve and exhaust port closed. Using the initial and boundary conditions as mentioned earlier, the computation proceeds with the piston descending downwards and the intake valve beginning to open so as to allow fluid to enter the flow domain, i.e. the cylinder. The closure of the intake valve (the passage between the valve and cylinder head is reduced to less than 0.25 mm) takes place in accordance with the actual valve timing of the engine. The intake valve closes at 64° after bottom centre (ABC), at which time the boundary condition at the intake valve is changed from 'pressure' to 'wall' to prevent fluid escaping from the cylinder. The valve closure is halted with a cell size of less than 0.25 mm to prevent collapse of the grid. In this transitional period, a lower time step of the order of 0.01° CA (1 ms) is adopted so as to prevent divergence in the solution. Further upward movement of the piston results in compression of the fluid till the piston reaches TC, beyond which fluid expansion occurs. The exhaust port is opened at 38° before bottom centre (BBC) by introducing a pressure boundary condition at the exhaust port. The exhaust process continues till the piston reaches TC, which completes one cycle of operation. Using the results of the first cycle as the initial condition, the second cycle is computed. This procedure is repeated to simulate operations at two CRs, 17 and 11.5. On the flat piston geometry, computations are attempted at CR = 17. Calculations are done with a grid density of 0.2 million cells. For a time step of 0.5° CA, the number of iterations employed to obtain a converged solution is about 70. The time step independence of the calculations has been verified, and this is shown in Figs 3 to 5. The principal parameters determined from these calculations are the velocity vectors at different time steps and the turbulence parameters, namely the turbulence intensity, u`, and the integral length scale, l_l. Turbulence is assumed to be isotropic, and therefore the turbulence intensity is calculated using the following correlation: turbulence kinetic energy = $3/2u'^2$.

7 CFD RESULTS

In this section, a schematic diagram derived from the velocity
profile across a selected plane is presented. Furthermore,
two-dimensional velocity vectors and a contour plot of the
scalar variable at time intervals close to TC are presented.
The flowfield related to bowl-in-piston geometry is mainly
discussed, and, at an important juncture, the result of flat
piston geometry is brought out in order to highlight the
features of geometry under investigation.

7.1 Velocity distribution

The flow during the induction is observed to be transient, highly turbulent and fluctuating. The evolving flow patterns as a function of time are schematically shown in Fig. 2, these are derived from the velocity profiles across the axial plane passing through the centre of the geometry. The schematic shown in the circumferential plane is below the cylinder head (1.2 mm), in the plane of the intake valve opening. The flow field is as follows. During the initial stages of the suction process, there are two major rotating flow patterns established in the cylinder as a consequence of the intake jet interacting with the walls of the cylinder. One flow pattern is termed 'swirl' (rotating mass about the cylinder axis) and occurs as the flow is discharged tangentially towards the cylinder wall, where it is deflected sideways and downwards in a swirling motion. The other flow pattern occupying the major part of the domain is observed in the transverse direction and is termed 'tumble' (rotating mass normal to the cylinder axis). Apart from these, there are recirculating flows in local regions in the vicinity of the cylinder head/bore interface, and these occur owing to flow separation. These are evident from Fig. 2 (at 30° CA) which shows the separation of the jet at the intake port and the setting up of a strong recirculating pattern at the corner of the geometry and also the commencement of tumbling flow vortices. The tumble flow consists of two barrel type vortices, which are observed to be asymmetric as against the symmetric vortices observed by Ekchian and Hoult [19] in water-analogy experiments.

This difference in the flow pattern is due to off-axis valve location in the current case as against the axisymmetric in-flow with Ekchian and Hoult [19]. The flow pattern in the case of an off-axis valve is much more complex, even though a similar structure is observed, and this is due to uneven flow distribution over the intake port cross-section.

The flow pattern at 60° CA corresponds to the piston approaching the maximum instantaneous speed. There are two vortices visible with different centres of rotation. The vortex away from the wall (right side) is rotating in the clockwise direction, with the centre of rotation close to the top of the piston. The second vortex is close to the wall (left side) and rotating in the counterclockwise direction, with the centre of rotation at a higher plane beneath the intake port. In addition, there is a distinct flow pattern visible in the bowl region. These vortices are continually convicted with the fluid as evident from the location of the centre of rotation of the left vortex corresponding to a piston position at 120° CA. It is also evident that the sense of rotation of the right-side vortex is reversed and is the same as that of the left-side vortex. These vortices further disintegrate and merge into a single vortex by the time the piston reaches the bottom centre (BC)—180° CA. Furthermore, during ascendance of the piston in the compression process, a single vortex in the cylindrical region is visible after the closure of the intake valve corresponding to 250° CA. The intensity of the swirling and the tumbling motion is normally quantified in terms of the swirl and tumble ratios. These are defined as

$$\text{Swirl ratio} = \frac{60H_y}{2\pi M_y N}$$

$$\text{Tumble ratio} = \frac{60H_{x,z}}{2\pi M_{x,z} N}$$

where $H_{x,y,z}$ and $M_{x,y,z}$ are the angular momentum and moment of inertia about the x, y, z axis respectively and N is the speed of the engine (r/min). These ratios change with the evolving flow pattern and are shown in Table 2 at particular crank angles. The tumble ratio is specified in the x and z planes about the instantaneous fluid centre of rotation, whereas the swirl ratio is computed about the y axis of

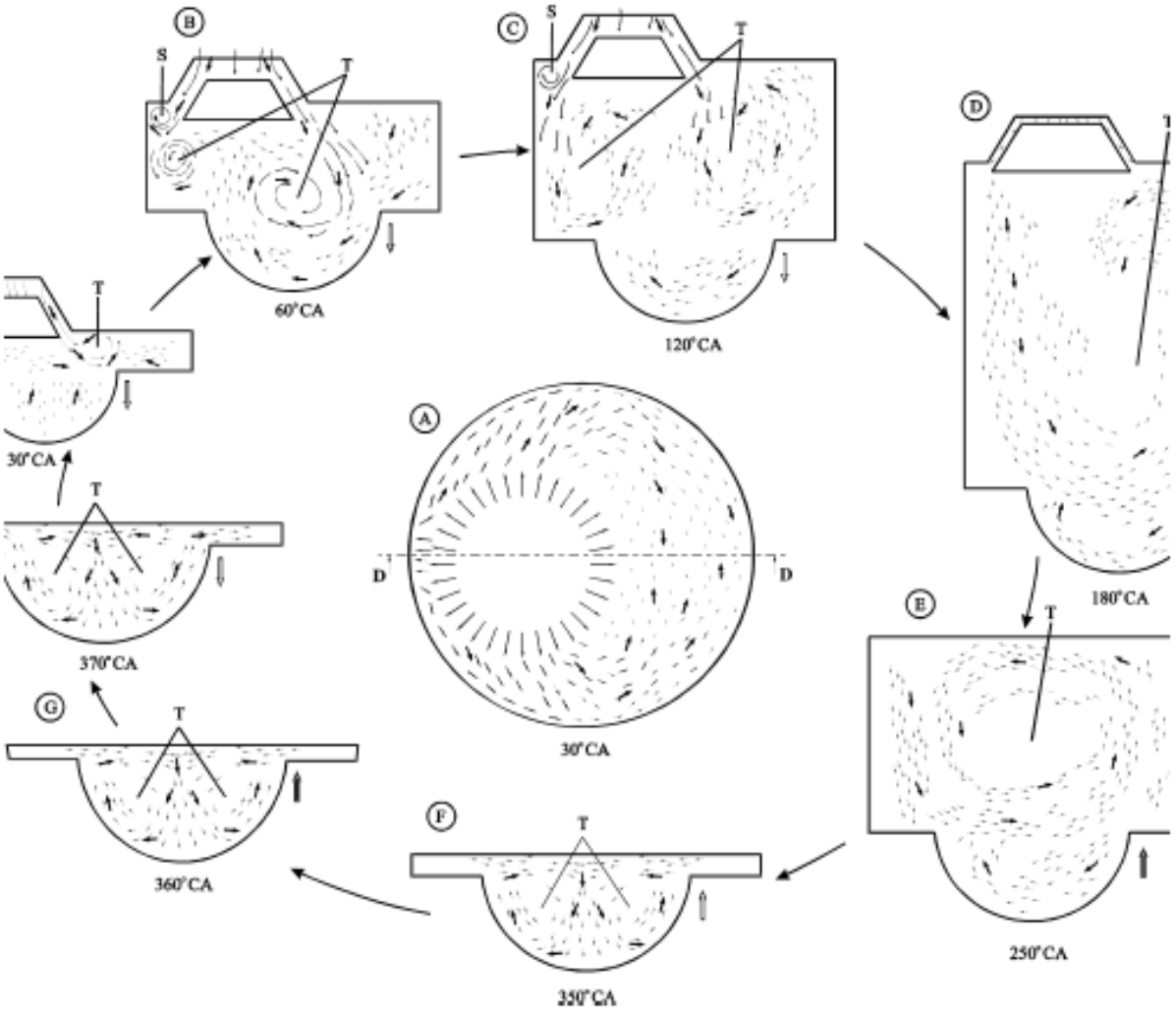

Fig. 2 Schematic diagram of the evolving fluid flow during intake, compression and the early part of expansion in a bowl-in-piston engine geometry. The central figure shows the tangential velocity plot in the circumferential plane, 1.2 mm below the intake valve. The axial view corresponds to the velocities along section DD. 'S' denotes the separation zone and 'T' denotes tumbling vortices. 360° CA corresponds to TC and 250° CA to flow after intake valve closure

the geometry or bowl axis. The swirl ratio is quantified at regular time intervals, but the tumble ratio is quantified in the event of a single tumble present in the flow domain, and this only occurs in the last stages of intake and the early part of the compression process.

As the piston ascends upwards during the compression process, the fluid from the cylindrical region is pushed into the bowl region, thereby increasing the angular velocity of the fluid in the bowl. The fluid flow pattern till the commencement of later part of the compression process is found to be same for both CRs. However, as the piston approaches TC (.330° CA), the squish affects fluid movement into the bowl and the squish velocities are found to be vastly different with the two CRs. Owing to the squish effect (which becomes dominant), the fluid in the cylindrical portion is pushed into the bowl, leading to the formation of two vortices in the bowl. The peak squish effect is observed around 350° CA, shown in Fig. 3, and the local velocities are as high as 20 m/s around the edge of the bowl, corresponding to CR = 17. There is a slight asymmetry in the velocity distribution, probably on account of the eccentricity of the

Table 2 Computed parameters at specific crank angles

CA (deg)	Swril Ratio* (y-axis)	Swril Ratio** (bowl axis)	Tumble ratio (x-axis)	Tumble ratio (z-axis)
180	1.00	1.60	1.35	1.35
250	0.85	1.41	1.50	1.50
270	0.90	1.45	1.40	1.40
300	0.82	1.63	1.20	1.20
330	0.50	1.10	NC	NC
360	0.30	0.40	NC	NC

* Complete Domain.
** Bowl region.
NC Not Calculated—regime of two tumbles.

bowl. The velocity vector plot in the axial plane at the same crank angle shows the evolution of counter-rotating toroidal vortices. At TC (360° CA) the counter-rotating vortices continue to survive and are displaced downwards in the bowl. These results are qualitatively compared with some of the experimental observations of Arcoumanis et al. [20] in Fig. 4. These researchers have experimentally measured the mean and turbulence velocities on an axisymmetric engine of CR = 6.7 at a speed of 200 r/min using three piston geometries, which include the bowl-in-piston geometry under motoring conditions.

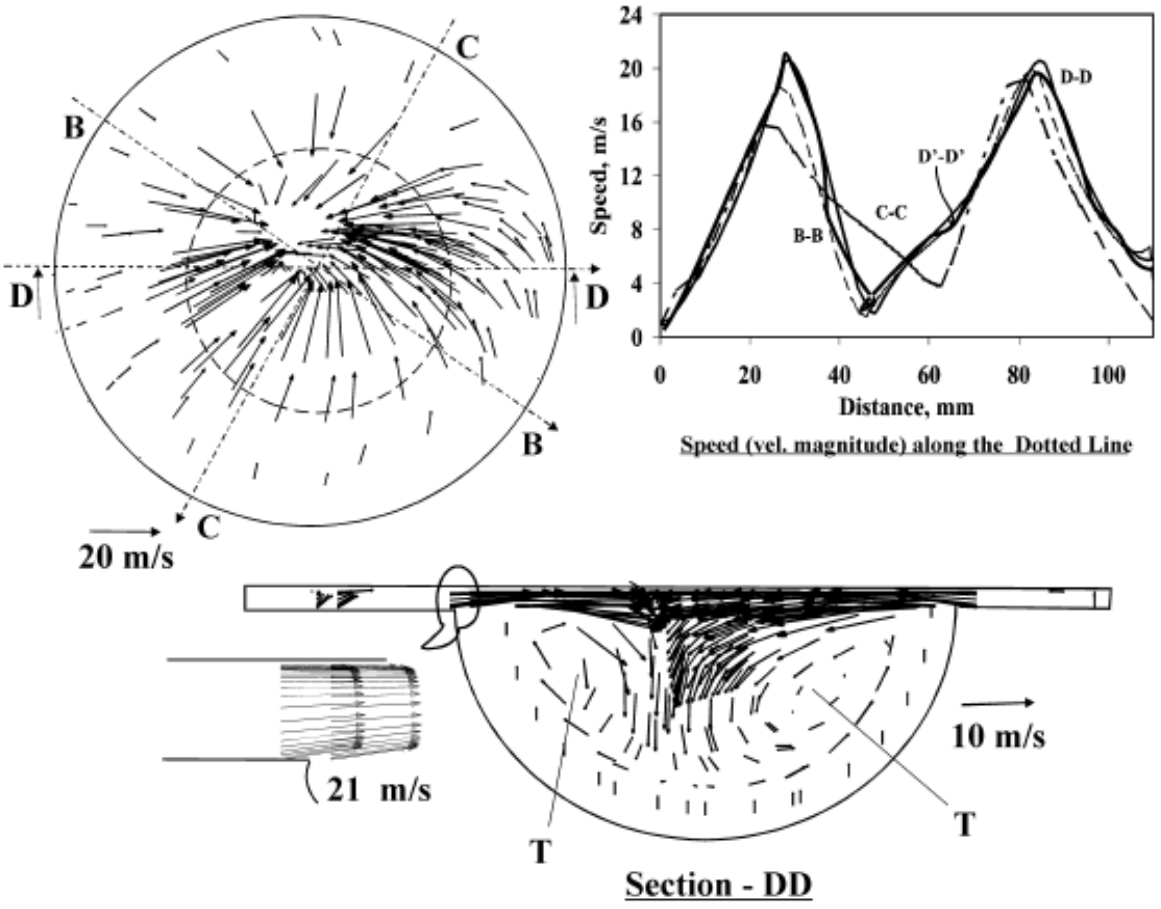

Fig. 3 All plots correspond to a time step of 0.5° CA, except for the curve D′–D′ (dark line) which corresponds to 1° CA. The vector plot in the axial plane (section DD) is for the squish period corresponding to 350° CA, CR = 17.0. The vector plot in the circumferential plane is at a distance of 1.2 mm below the cylinder head, and the dashed circle in the circumferential view represents the edge of the bowl

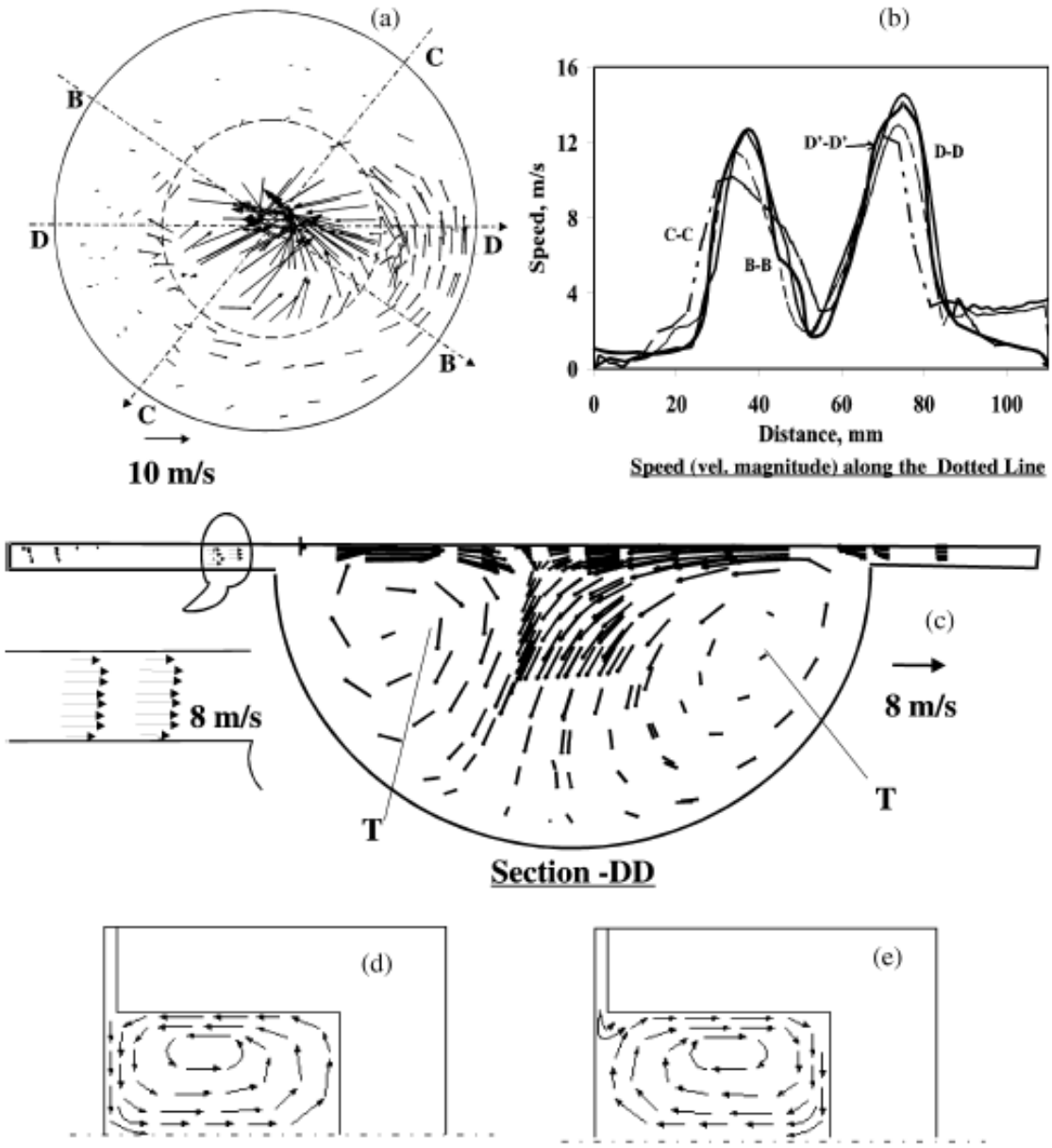

Fig. 4 All plots corresponds to a time step of 0.5° CA, except for the curve D′-D′(dark line) in Fig. 4b which corresponds to 1° CA: (a) vector plot in the circumferential plane is at a distance of 1.2 mm below the cylinder head corresponding to 360° CA (TC), CR = 17.0; (b) speed along the dotted line; (c) velocity in the axial plane (section DD); (d) and (e) experimental results about the symmetry plane from reference [20] at 360°CA (TC) in the absence and presence of intake swirl respectively. The dashed circle represents the edge of the bowl

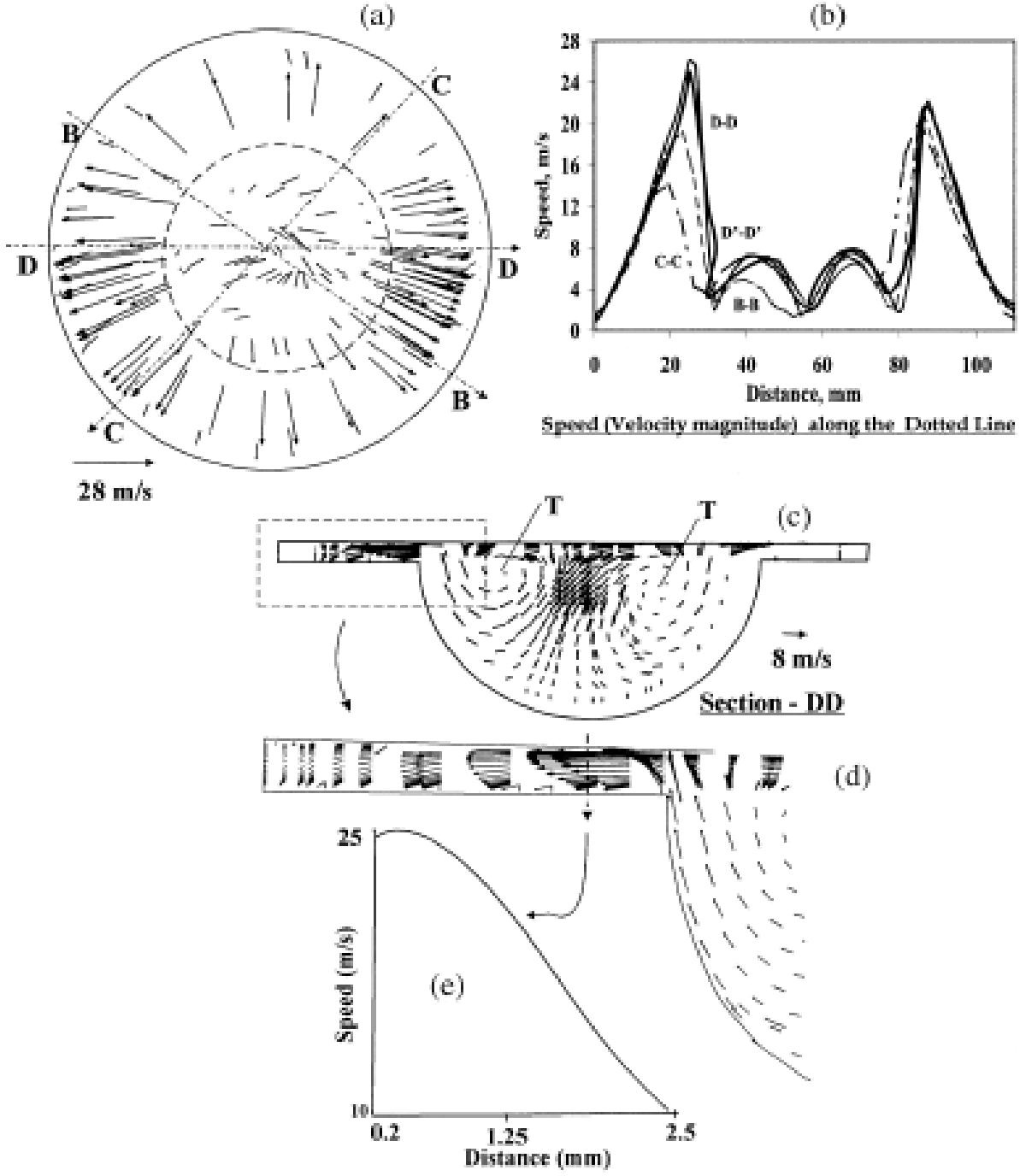

Fig. 5 All plots correspond to a time step of 0.58 CA, except the curve D′–D′ (dark line) in Fig. 5b which corresponds to 1° CA: (a) vector plot in the circumferential plane at a distance of 1.2 mm below the cylinder head corresponding to 370° CA, CR = 17.0; (b) speed along the dotted line; (c) velocity in the axial plane (section DD); (d) enlarged view of the velocity plot near the edge of the bowl; (e) speed in the axial direction along the dotted line shown in (d). The dashed circle represents the edge of the bowl

Measurements are reported to have been done in the presence and absence of swirl so as to access its influence on the mean and turbulence velocities. The predicted flowfield pattern compares favourably (in the sense of vortex rotation) with the experimental results observed in the absence of intake swirl. However, the CFD result shows the existence of swirl during the intake process (peak swirl ratio ~2.1 at 50° CA). Further comparison with the experimental flowfield in the presence of intake swirl (opposite sense of rotation of the vortex, shown in Fig. 4e) would not be appropriate because the mean piston speed in the two cases is widely different (0.63 m/s in experiments as against 5.8 m/s in CFD) and, with squish velocity being linearly dependent on piston speed [21], it is conjectured that the behaviour would be vastly different in the two cases.

The swirl ratio at the end of the compression process is quantified as 0.3; this reduction in swirl could be due to interaction of the swirl with the squish. Furthermore, as the piston descends downwards from TC, the effect of reverse squish sets in, where the fluid begins to flow out of the bowl into the cylindrical region and, in the process the counter-rotating vortices are displaced upwards. Here, it is necessary to emphasize that the reverse squish effect is vastly different with the two CRs which is discussed later in this section. The fluid movement further intensifies with the piston descending downwards as shown in Fig. 5, and the maximum reverse squish effect becomes evident at about 370–372° CA, where the velocities are as high as 31 m/s with asymmetry in the velocity distribution. At CR=11.5, the observed flow field is similar to that at 17.0 CR. However, the squish and reverse squish velocities are lower, corresponding to CR= 17.0. The peak squish velocities are in the range of 8 m/s at 3508 CA. Similarly, the fluid movement out of the bowl during the reverse squish period is not intense, and the maximum velocity at the edge of the bowl is of the order of 5–6 m/s with asymmetry in the distribution, as evident from Fig. 6.

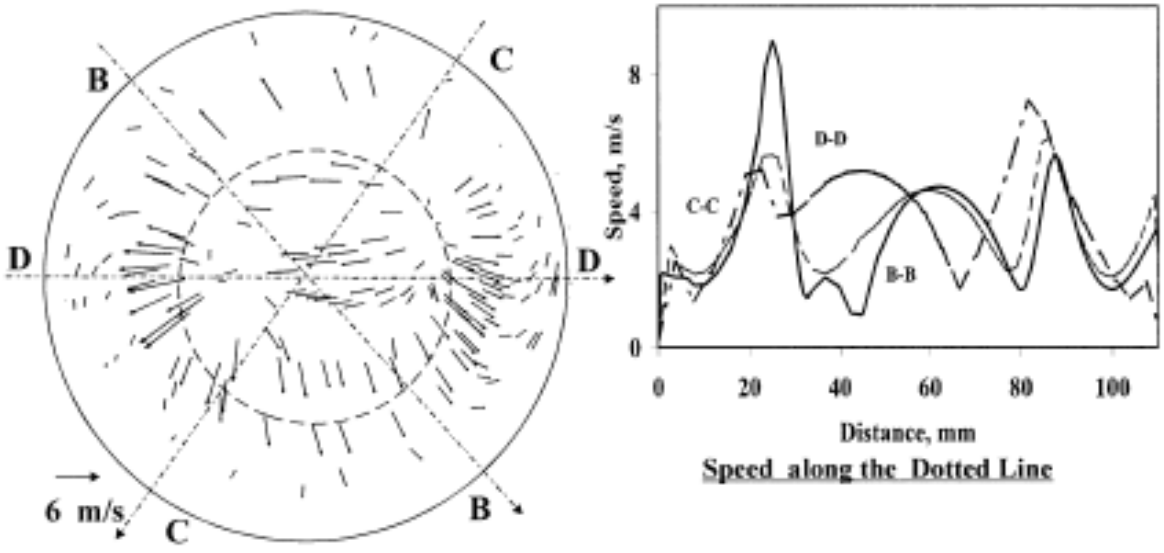

Fig. 6 Vector plot in the circumferential plane at a distance of 1.2 mm below the cylinder head corresponding to 370° CA, CR = 11.5. The dotted circle represents the edge of the bowl

With regard to the flat piston geometry, the fluid flow indicates the presence of a single vortex, as shown in Fig. 7a, at the completion of valve closure, with swirl and tumble ratios of 0.85 and 1.3 respectively, comparing closely with the bowl geometry. However, in the later part of the compression process there is no evidence of tumbling flow, as shown in Fig. 7b. The resultant flowfield close to TC has an influence on the turbulence intensity, which will be discussed below.

Summarizing the flowfield results, the jet-like character of the intake flow interacting with the cylinder walls and the moving piston creates a large-scale rotating flow pattern within the cylinder. The flowfield is observed to undergo large-scale changes during intake and subsequently in the compression process. Between the two CRs with bowl-in-piston geometry there is no distinct change in the fluid flow pattern in the intake and early part of the compression process. However, in the last stages of compression and the early part of expansion, the fluid velocities near the edge of the bowl are largely different, the high CR creating large shear zones near to the edge of the bowl.

Between the flat head and bowl-in-piston geometries, the swirl and tumble ratios are about the same during the intake process. During compression, the swirl ratio is found to be higher in the bowl region owing to increase in the angular velocity of the fluid. However, there is one distinct difference observed between the two geometries:

1. In the case of bowl-in-piston geometries there is evidence of the formation of two tumbling vortices, and these survive till TC.
2. In the flat piston geometry there is evidence of a single tumbling vortex during the early part of the compression, and this is dissipated much earlier than the completion of the compression process.

The effect of these flow patterns on the turbulence generation is discussed below.

7.2 Turbulence distribution

The variation in turbulence intensity, u′, and integral length scale, l_l will be discussed first. Further insight is provided by examining the spatial distribution of turbulence kinetic energy in and around TC, which is relevant from the combustion viewpoint. Figure 8 shows the CFD results of u′ values for the bowl-in piston geometry in the diametric plane (4 mm below the cylinder head). The computed results are shown with and without the compressibility effects in the 1 equation. Examination of the computed results reveals large variation in u′ right through the induction and compression process. Initial high turbulence sets in

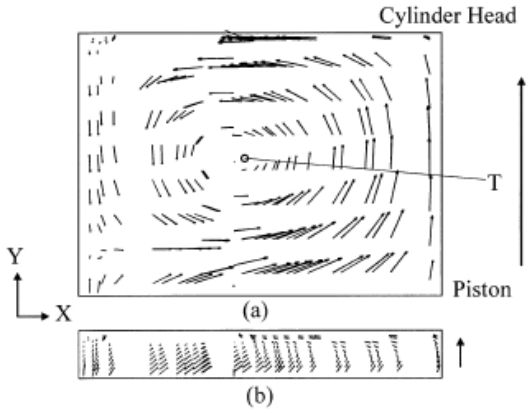

Fig. 7 Vector plot in the axial plane with flat piston geometry (CR = 17.0): (a) 250° CA, (b) 330° CA

owing to shear in the high-velocity jet entering the cylinder. The turbulence fluctuation, u′, goes to as high as 22 m/s, and this approximately coincides with the point of maximum piston speed and the valve lift, further to which there is a fall in turbulence intensity with commencement of intake valve closure. The turbulence fluctuation, u′, again increases beyond the intake valve closure owing to increased fluid movement, and it peaks at about 30° CA prior to TC, subsequent to which there is a decline. These results are comparable with and without allowance for the compressibility effect in the 1 equation.

Furthermore, the results are compared with the experimental results of Catania and spessa [22], as shown in Fig. 8. These experiments are conducted on a production diesel engine of CR=18.0, with slightly re-entrant bowl-in piston geometry using a hot-wire anemometer at a varying speed ranging between 600 and 3000 r/min. The comparison is made considering the results at two engine speeds, namely 1500 and 2000 r/min, which correspond to two mean piston speeds of 4.3 and 5.8 m/s. The comparison of the u0 between the two results appears fair (considering the fact that the geometries are similar but not identical) till about inlet valve closure. In this time period, the location of the peak value is different by about 30–40° CA, and this is attributed to differences in intake valve timing/valve lift profile. Beyond the intake valve closure, opposing trends in the variation of u′ with CA are found. As the piston starts compressing the fluid, there is an increase in u0, which peaks at 30° BTC, beyond which there is a decline in u0 against a continuous decline in the measured values. In the post-TC region, there is again a contradictory trend by comparison with experimental results. This feature is unaltered even when the compressibility effect is accounted for by choosing a constant of 20.373 [18] for the velocity dilatation term in the 1 equation. A similar solution is obtained adapting a finer grid of 0.27 and 0.34 million

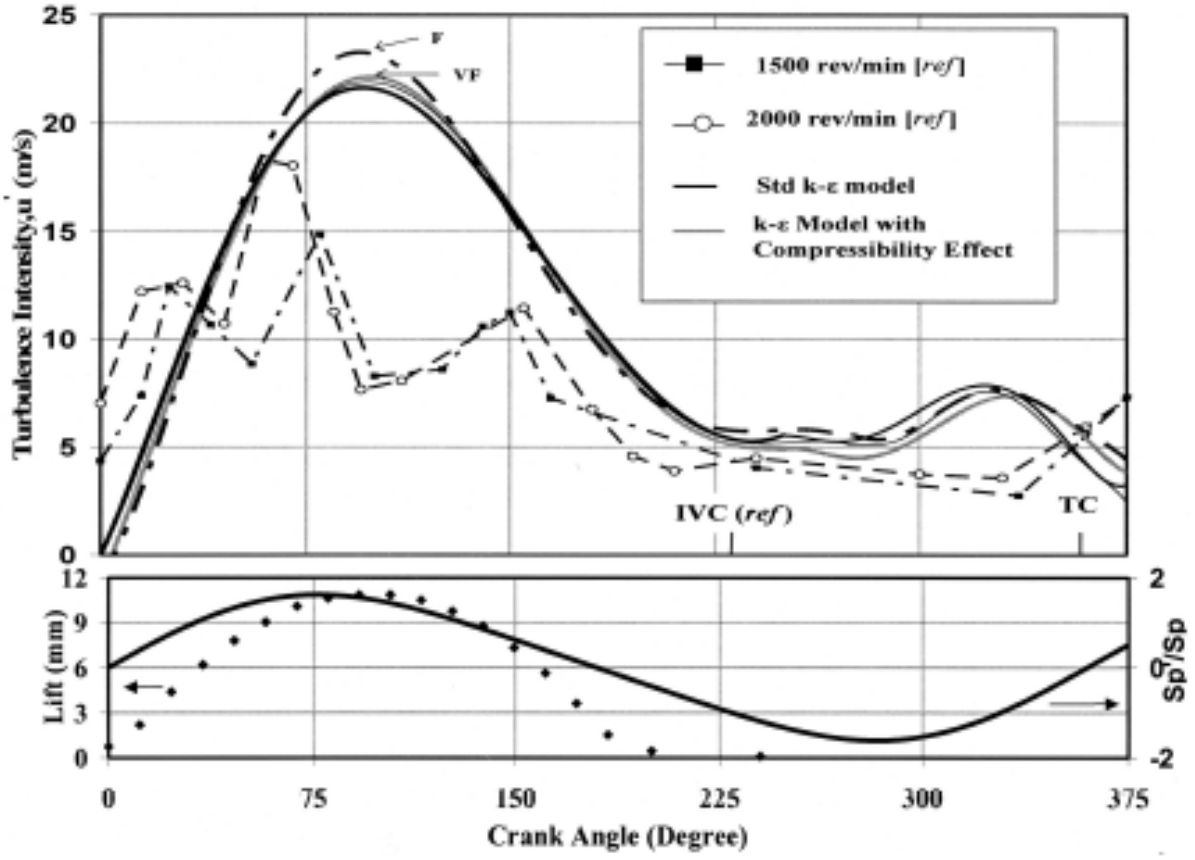

Fig. 8 Top plot is the CFD result using the k – ε Model (with and without the compressibility effect) as a function of crank angle using 0.2 million cells; F and VF refer to computations with 0.27 and 0.34 million cells by including the compressibility effect. *ref* is the experimental result of Catania and Spessa [22] on a similar configuration engine. The bottom plot (solid line) shows the variation in instantaneous piston speed normalized with the mean piston speed (5.8 m/s) for the CFD geometry and corresponding to 2000 r/min of *ref.* The dotted line is the intake valve lift profile of the CFD geometry. The maximum intake valve lift for ref is 8.1 mm

cells, and therefore the solution obtained above is essentially grid independent. In the work of Han and Reitz [16], using the RNG k–ε model on a Mexican hat piston top where the effect of velocity dilatation and kinematic viscosity are accounted for in the 1 equation, similar qualitative behaviour of u′ declining in the post-TC period, as noted here, has been observed. However, other experimental studies in the literature suggest a trend of increase in u′ for certain bowl-in-piston geometries, namely a re-entrant configuration compared with a simpler cylindrical configuration in the post-TC period [23], and this is taken as being due to higher shear zones with re-entrant geometries. Coming to the present comparison, even though the bowl geometries are different, nevertheless a similar trend in the turbulence intensity behaviour is expected considering the bowl shape in the experimental work [22] not to be of the completely re-entrant type. Therefore, this discrepancy in the trends could only be attributed to the limitation of the k–ε turbulence model in capturing the transient effects around TC, where squish and reverse squish effects are dominant.

Next, the mass-averaged u′ and l_I as a function of CR are shown in Fig. 9, where the location corresponds to the mid three-dimensional zone in the bowl region of the geometry. These time-varying mass-averaged data have been used as a representative value in zero-dimensional thermodynamic modelling for making pressure–crank angle predictions, by

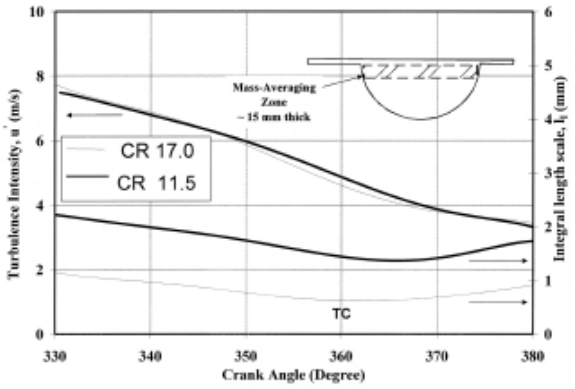

Fig. 9 Variation in mass-averaged u′ and l_I across a three dimensional zone shown in the inset at varying CRs

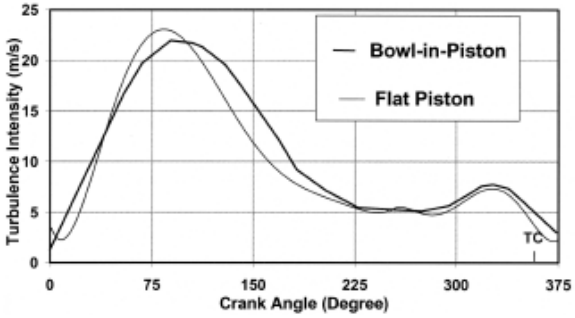

Fig. 10 Comparison of u′ for the two piston geometries—4 mm below the cylinder head

considering a simple rapid distortion process to account for reaction conditions in earlier work by the present authors [13, 14]. It is clear from the figure that variation in u′ with time is close to being independent of CR; this is consistent with the observations made by Lancaster [24] and Ikegami et al. [25]. Similarly, the variation in lI calculated using k and ε is also shown in Fig. 9, which indicates l_I to be higher at lower CR compared with higher CR and is qualitatively consistent with the experimental results of Ikegami et al. [25]. Figure 10 shows the comparison of u′ for both piston geometries. The variation in u0 with time is about the same until the early part of the compression process. In the later part of the compression process, it is evident that decline in u′ is faster in the case of the flat geometry. This declining behaviour could be due to the following factors:

a) The absence of a squish-generating mechanism with flat geometry,
b) The absence of tumbling vortices in the later part of the compression process.

The absence of a turbulence-generating mechanism such as squish in the case of flat geometry is evident. However, it is important to recognize the role of the tumbling vortices, taking note of the literature. Floch et al. [26] have studied the influence of swirl and tumble on the turbulence intensity and combustion in an SI engine. Their study indicates the breakdown of the tumbling vortices (prior to TC) to be responsible for enhancement of turbulence along with decline in the tangential velocities. It is conjectured that tumble contributes to higher turbulence owing to the dissociation of the main vortex into turbulence

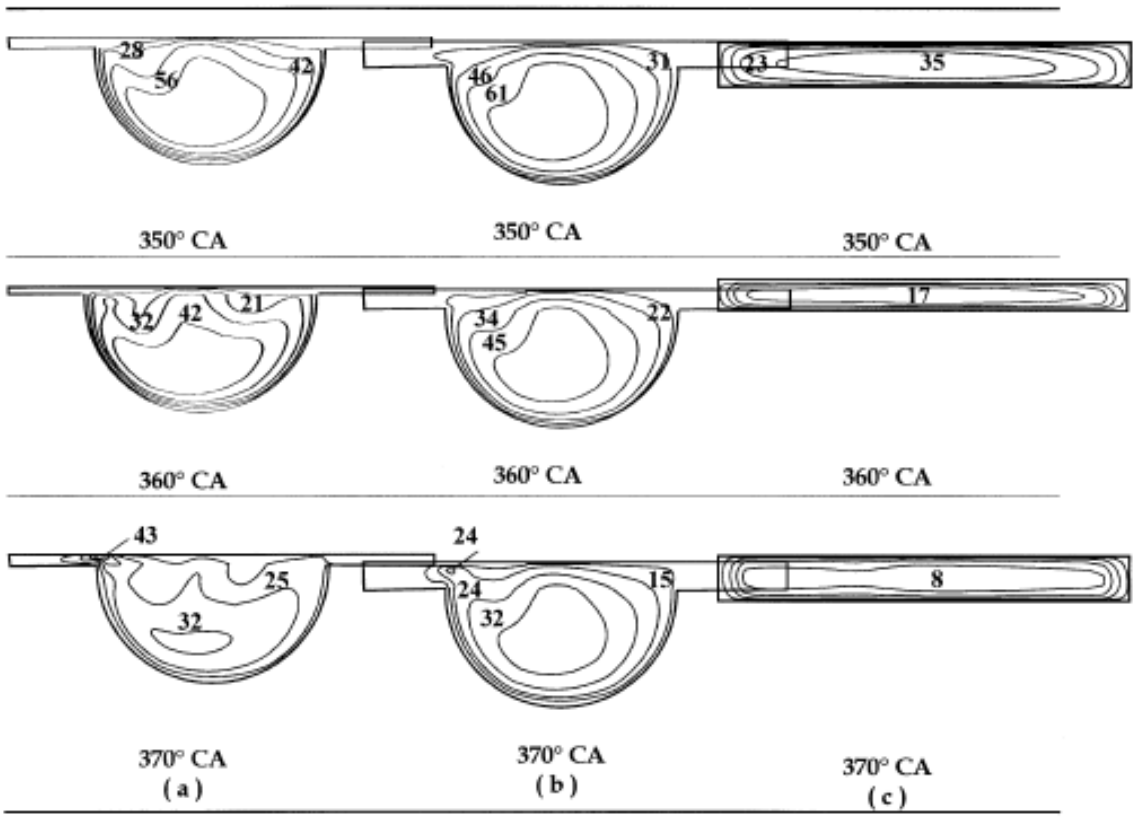

Fig. 11 CFD results: contour plot of turbulence kinetic energy (m^2/s^2) on an axial plane through the centre of the geometry—the same as plane D–D in Fig. 3 (close to the spark plug location): (a) bowl geometry, CR = 17.0; (b) bowl geometry, CR = 11.5; (c) flat geometry, CR = 17

as a result of piston movement. It is further observed that, in the case of swirl, the rotating motion is conserved during the compression process, thereby contributing to turbulence generation to a lesser extent (on account of lesser swirl dissociation). Similarly, Urushihara et al. [27] observe that tumble flow generates turbulence in the combustion chamber more effectively than swirl flow does, and that swirling motion reduces the cycle-by-cycle variation in mean velocity that tends to be generated by the tumbling motion. In the present study there is evidence of tumble vortex breakdown with flat piston geometry much earlier than TC, and this, apart from the absence of squish, appears to be responsible for the faster decline in u′

Next, the spatial distribution of turbulence kinetic energy (TKE) at crank angles close to TC for both CRs and for the flat piston geometry is shown in Fig. 11. The contour plots in the axial plane reveal spatial variation in TKE, which is consistent with the experimental observations of Schapertons and Thiele [4]. A general observation at all time steps indicates the TKE to be of high intensity in the central region of the bowl, decreasing towards the walls. Further revealing information from the contour plot is the shift in the distribution of TKE with time, which is caused by changes in the flow pattern in the bowl region owing to squish and reverse squish effects. It is also observed that the TKE is marginally lower (5 per cent) at higher CR, probably owing to enhanced dissipation of kinetic energy on account of increased fluid movement during the squish and reverse squish period. Lastly, comparison of the TKE of the two piston geometries reveals substantial enhanced TKE for bowl-in-piston geometry compared with the flat piston. In the case of flat geometry, the TKE is more or less uniform throughout the combustion chamber.

8 CONCLUSION

Three-dimensional computations on engine geometry are able to capture the generic features of fluid flow in a reciprocating engine and are consistent with some of the experimental observations available in the literature. The presence of high shear zones near to the edge of the bowl during squish/reverse squish is evident, more so in the case of the higher CR with bowl-in-piston geometry. The standard k–ε model predicts trends in turbulence intensity around TC that are different from the experimental data available in the literature. This is thought to be due to limitation of the k–ε model in capturing the transient effects during the squish/reverse squish period and therefore not attributable to difference in shape of the combustion chamber geometry.

These motored turbulence parameters, namely the turbulence intensity and length scale, have been used as input for zero-dimensional thermodynamic modelling by considering a simple rapid distortion process to account for reaction conditions in earlier publications [13, 14]. The zero-dimensional modelling is able to make reasonably accurate predictions at advanced ignition timing; here, the predicted pressure–crank angle curve matches reasonably well with the experimental results obtained on a high compression ratio gas engine with biomass-derived producer gas as the fuel [15]. However, at the optimum ignition setting (typically less than 108 BTC), the predictions are inaccurate when the reverse squish effect becomes dominant. It appears that the enhanced fluid movement during the reverse squish period (evident from the CFD study) significantly modifies the burn rate. However, it might be possible to gain insight into some of these aspects more precisely by adapting computational techniques such as LES.

REFERENCES

1. Versteeg, H.K. and Malalasekhara, W. An Introduction to CFD—The Finite Volume ethod, 1995 (Longman Scientific and Technical). Q1

2. Lebrere, L. and Dillies, B. Engine flow calculations using a Reynolds stress model in the Kiva-II code. SAE paper 960636, 1996, Vol. 105, pp. 882–904.

3. Watkins, A.P., Li, S.-P. and Cant, R.S. Premixed combustion modeling for SI engine applications. SAE paper 961190, 1996, Vol. 105, pp. 1614–1626.

4. Schapertons, H. and Thiele, F. Three dimensional computations for flow fields in DI piston bowls. SAE paper 860463, 1986, Vol. 95, pp. 135–15. Q2

5. Haworth, D.C., Sherif, H., Tahry, E.I., Huebler, M.S. and Chang, S. Multidimensional port-and-cylinder for two- and four-valve-per-cylinder engines: influence of intake configuration on flow structure. SAE paper 900257, 1990, Vol. 99, pp. 647–675.

6. Trigui, N., Affes, H. and Kent, J.C. Use of experimentally measured in-cylinder flow field data at IVC as initial conditions to CFD simulations of compression stroke in I.C. engines—a feasibility study. SAE paper 940280, 1994, Vol. 103, pp. 343–352.

7. Jones, P. and Junds, J.S. Full cycle computational fluid dynamics calculations in a motored four valve pent roof combustion chamber and comparison with experiments. SAE paper 950282, 1995, Vol. 104, pp. 595–610.

8. Strauss, T.S., Schweimer, G.W. and Ritscher, U. Combustion in a swirl chamber diesel engine simulation by computation of fluid dynamics. SAE paper 950280, 1995, Vol. 104, pp. 519–530.

9. Reuss, D.L., Kuo, T.W., Khalighi, B., Haworth, D. and Rosalik, M. Particle image velocimetry measurements in a high-swirl engine used for evaluation of computational fluid dynamics calculations. SAE paper 952381, 1995, Vol. 104, pp. 2073–2092.

10. Khalighi, B., El Tahry, S.H., Haworth, D.C. and Huebler, M.S. Computation

and measurement of flow and combustion in a four-valve engine with intake variations. SAE paper 950287, 1995, Vol. 104, pp. 611–644. Q3

11. Bauer, W., Heywood, J.B., Avanessian, O. and Chu, D. Flow characteristics in intake port of spark ignition engine investigated by CFD and transient gas temperature measurements. SAE paper 961997, 1996, Vol. 105, pp. 2110–2117.

12. Duclos, J.M., Bruneaux, G. and Baritaud, T.A. 3D modeling of combustion and pollutants in a 4-valve SI engine; effect of fuel and residuals distribution and spark location. SAE paper 961964, 1996, Vol. 105, pp. 2048–2062.

13. Sridhar, G., Paul, P.J. and Mukunda, H.S. Experiments and modelling of producer gas based reciprocating engines. In Proceedings of 2002 Fall Technical Conference of ASME Internal Combustion Engines Division, New Orleans, Louisiana, 2002, ICE-Vol. 39, paper no. ICEF2002-520, pp. 377–388.

14. Sridhar, G. Experimental and modelling studies of producer gas based spark-ignited reciprocating engines. PhD thesis, Indian Institute of Science, 2003.

15. Sridhar, G., Paul, P.J. and Mukunda, H.S. Biomass derived producer gas as a reciprocating engine fuel—an experimental analysis. Biomass and Bioenergy, 2001, 21, 61–72.

16. Han, Z. and Reitz, R.D. Turbulence modeling of internal combustion engines using RNG k-1 model. Combustion Sci. Technol., 1995, 106, pp. 267–295.

17. Hawkins, I.R. and Wilkes, N.S. Moving grids in HARWELLFLOW3D. AEA-InTec-0608, 1991.

18. Jennings, M.J. Multi-dimensional modeling of turbulent pre-mixed charge combustion. SAE paper 920589, 1992, Vol. 101, pp. 1106–1124.

19. Ekchian, A. and Hoult, D.P. Flow visualization study of intake process of an internal combustion engine. SAE paper 790095, 1979, Vol. 88, pp. 383–399.

20. Arcoumanis, C., Bicen, A.F. and Whitelaw, J.H. Squish and swirl–squish interaction in motored model engines. Trans. ASME J. Fluid Engng, 1983, 105, 105–112.

21. Heywood, J.B. Internal Combustion Engine Fundamentals, international edition, 1988 (McGraw-Hill). Q4

22. Catania, A.E. and Spessa, E. Speed dependence of turbulence properties in a high-squish automotive engine combustion system, SAE paper 960268, 1996, Vol. 105, pp. 313–334.

23. Corcione, F.E. and Valentino, G.Analysis of in-cylinder flow processes by LDA. Combustion and Flame, 1994, 99, pp. 387–394.

24. Lancaster, D.R. Effects of engine variables on turbulence in a spark-ignition engine. SAE paper 760159, 1976, Vol. 85, pp. 671–688.

25. Ikegami, M., Shioji, M. and Nishimoto, K. Turbulence intensity and spatial integral scale during compression and expansion strokes in a four cycle reciprocating engine. SAE paper 870372, 1987, Vol. 96, pp. 4.399–4.441.

26. Floch, A., Franck, J.V. and Ahmed, A. Comparison of the effects of intake generated swirl and tumble on turbulence characteristic in a 4-valve engine. SAE paper 952457, 1995,Vol. 104, pp. 2239–2255.

27. Urushihara, T., Murayama, T., Takagi, Y. and Lee, K.-H. Turbulence and cycle-by-cycle variation of mean velocity generated by swirl and tumble flow and their effects on combustion. SAE paper 950813, 1995, Vol. 104, pp. 1382–1389.